Published in final edited form as:
J Am Chem Soc. 2002 October 16; 124(41): 12302–12311.

How Ions Affect the Structure of Water

Barbara Hribar[†], **Noel T. Southall**[‡], **Vojko Vlachy**[†], and **Ken A. Dill**[*,§]
Contribution from the Faculty of Chemistry and Chemical Technology, University of Ljubljana, Askerèeva 5, 1000 Ljubljana, Slovenia, Graduate Group in Biophysics, University of California, San Francisco, California 94143-1204, and Department of Pharmaceutical Chemistry and Graduate Group in Biophysics, University of California, San Francisco, California 94143-1204

Abstract

We model ion solvation in water. We use the MB model of water, a simple two-dimensional statistical mechanical model in which waters are represented as Lennard-Jones disks having Gaussian hydrogen-bonding arms. We introduce a charge dipole into MB waters. We perform (NPT) Monte Carlo simulations to explore how water molecules are organized around ions and around nonpolar solutes in salt solutions. The model gives good qualitative agreement with experiments, including Jones–Dole viscosity *B* coefficients, Samoilov and Hirata ion hydration activation energies, ion solvation thermodynamics, and Setschenow coefficients for Hofmeister series ions, which describe the salt concentration dependence of the solubilities of hydrophobic solutes. The two main ideas captured here are (1) that charge densities govern the interactions of ions with water, and (2) that a balance of forces determines water structure: electrostatics (water's dipole interacting with ions) and hydrogen bonding (water interacting with neighboring waters). Small ions (kosmotropes) have high charge densities so they cause strong electrostatic ordering of nearby waters, breaking hydrogen bonds. In contrast, large ions (chaotropes) have low charge densities, and surrounding water molecules are largely hydrogen bonded.

1. Introduction

Ion–water interactions are important throughout biology and chemistry. Ions affect the conformations and activities of proteins and nucleic acids[1–3] and the specificity of ion binding. Ion complexation in cells is crucial for the activities of biomolecules such as enzymes and drugs.[4,5] Ions regulate the electrostatic potentials, conductances, and permeabilities of cell membranes,[6,7] the structures of micelles, and the hydrophobic effect (called Hofmeister effects), which drives partitioning, permeation, and folding and binding processes.[8,9] In chemistry, ions affect the rates of chemical reactions;[10,11] rates of gelation, widely used in food applications;[12] ion-exchange mechanisms, widely used for chemical separations;[13] and the expansion and contraction of clays, responsible for environmental processes such as mudslides.[14] Ion hydration has been studied extensively, both experimentally[15–19] and theoretically.[20–25]

Ions have long been classified as being either kosmotropes (structure makers) or chaotropes (structure breakers) according to their relative abilities to induce the structuring of water. The degree of water structuring is determined mainly by two types of quantities: the increase or decrease in viscosity in water due to added salt, and entropies of ion solvation. For example,

* To whom correspondence should be addressed. E-mail: dill@zimm.ucsf.edu..
[†]University of Ljubljana.
[‡]Graduate Group in Biophysics, University of California.
[§]Department of Pharmaceutical Chemistry and Graduate Group in Biophysics, University of California.

the viscosity η of an aqueous salt solution typically has the following dependence on ion concentration *c*:[18]

$$\eta / \eta_0 = 1 + Ac^{1/2} + Bc + \ldots \quad (1)$$

where η_0 is the viscosity of pure water at the same temperature. *A* is a constant independent of *c*; its corresponding term can be explained by Debye–Hückel theory as being due to counterion screening at low ion concentrations. The constant *B*, which is called the Jones–Dole *B* coefficient, is the quantity that defines the degree of water structuring of interest here.[18] *B* is positive for kosmotropic ions and negative for chaotropic ions. One issue in interpreting experiments is how to separate the contributions of the anion from the cation. The standard assumption is that K^+ has the same *B* coefficient as Cl^-, $B_{K^+} = B_{Cl^-}$, because K^+ and Cl^- have approximately the same ionic conductances[26] and because the value of *B* for KCl is approximately zero.

Water structuring is also reflected in entropies of ion solvation. To obtain these entropies, two assumptions are commonly used. First, to separate the effects of the anion from the cation, it is assumed that the solvation entropies are additive.[17] Second, an assumption is required to parse the ion solvation entropy into components due to the ion and due to water. By splitting the solvation entropy, ΔS^{hyd}, into ion and hydration water contributions and subtracting the former, ΔS_{II} is obtained, which describes the change in entropy of hydration water due to the presence of an ion.[17] Ions which are kosmotropic in viscosity experiments tend to have a negative hydration component to their solvation entropy, implying that they order the nearby waters, while chaotropic ions have a positive ΔS_{II}.

The experiments show that water is ordered by small or multivalent ions and disordered by large monovalent ions. Therefore, water ordering has generally been interpreted in terms of ion charge densities.[17,27] Charge densities are high on ions that have a small radius and/or a large charge.

A related property is the Hofmeister effect.[28] In 1888, Hofmeister reported that salts affect the solubilities of proteins in water to varying degrees. This has been interpreted as a modulation of the hydrophobic effect by salts because it is also found that increasing salt concentration reduces the solubilities of simple hydrophobic solutes such as benzene in aqueous solutions.[29,30] The Hofmeister series is a list of ions rank-ordered in terms of how strongly they modulate hydrophobicity. Such salt effects on nonpolar solubilities correlate with charge densities of the salts. Small ions tend to cause “salting out”, that is, to reduce hydrophobic solubilities in water, whereas large ions tend to cause “salting-in”, increasing nonpolar solubilities. The Hofmeister series, however, does not correlate perfectly with ionic charge density: while lithium is smaller than sodium, lithium has a weaker Hofmeister effect.

The Hofmeister effect is directly proportional to salt concentration and modeled by the Setschenow equation:[31]

$$\ln [c_i / c_i(0)] = -k_s c_s \quad (2)$$

where c_i and $c_i(0)$ are the molar solubilities of the hydrophobe in a salt solution and water, respectively, c_s is the molar concentration of the salt, and k_s is the salt’s Setschenow salting-out coefficient.

There are various microscopic perspectives on these properties. Smith[32] and Kalra et al.[33] have calculated Setschenow coefficients from molecular dynamics simulations. In their

simulations, the hydrophobe–ion pair distribution functions show that strongly salting-out (small) ions are generally excluded from the nonpolar solute's first water shell.

In 1957, Samoilov[15,16] proposed that dynamic properties, such as the viscosity, could be understood in terms of the activation energy required to strip a water molecule away from the first solvation shell of an ion as compared to that for another water, $\Delta E_i = E_i - E_0$. E_0 is the activation energy for the process of transferring a water molecule from a first shell around another water molecule to its next coordination shell, and E_i is the corresponding activation energy for a water molecule in an ion coordination shell.[15] A water molecule "binds" to a small ion more tightly than it binds to a neighboring water molecule, resulting in a positive activation energy, while water molecules next to big ions are more mobile than bulk water molecules ($\Delta E_i < 0$).

Collins[27] proposed that ion effects on water structure could be explained by a competition between ion–water interactions, which are dominated by charge density effects, and water–water interactions, which are dominated by hydrogen bonding. He explained that anions are stronger than cations at water ordering because of the asymmetry of charge in a water molecule: the negative end of water's dipole is nearer to the center of the water molecule than the positive end. Therefore, anions see a larger electrostatic potential at the surface of a water molecule than cations see. Our preliminary calculations indicate[34] that the solvation model of Collins yields qualitative agreement with the experimental data. We were motivated by Collins' insightful qualitative model to make a more quantitative statistical mechanical model.

2. The Model and Simulation

We wanted a model that (1) is physical, that is, based on an energy function related to the structure of water, and (2) is computationally efficient enough to sample the spatial and energetic distributions of water molecules. High-resolution all-atom simulations are computationally intensive, particularly for studies, such as Hofmeister effects, that involve three species: water, ion, and nonpolar solute. Here we use the MB model, in which each water molecule is represented as a two-dimensional disk that interacts with other waters through a Lennard-Jones (LJ) interaction and through an orientation-dependent hydrogen-bonding (HB) interaction. The name "MB" arises because there are three hydrogen-bonding arms, arranged as in the Mercedes Benz logo (Figure 1). There are various anomalous properties of pure water[35–39] including the density anomaly, a minimum in isothermal compressibility, and a large heat capacity; they are reproduced qualitatively by the MB model.[40] The model also captures qualitatively the properties of the water as a solvent for nonpolar solutes[41,42] – the hydrophobic effect.[40,43]

In the MB model, the energy of interaction between two waters is

$$U^{WW}(\boldsymbol{X}_i, \boldsymbol{X}_j) = U_{LJ}(r_{ij}) + U_{HB}(\boldsymbol{X}_i, \boldsymbol{X}_j) \tag{3}$$

The notation is the same as in previous papers: $\mathbf{X}_i$ denotes a vector representing both the coordinates and the orientation of the ith water molecule, and r_{ij} is the distance between the molecular centers of molecules i and j. The LJ term is

$$U_{LJ}(r_{ij}) = 4\varepsilon_{LJ}\left[\left(\frac{\sigma_{LJ}}{r_{ij}}\right)^{12} - \left(\frac{\sigma_{LJ}}{r_{ij}}\right)^{6}\right] \tag{4}$$

where ε_{LJ} and σ_{LJ} are the well-depth and contact parameters, respectively. In addition, neighboring water molecules form an explicit hydrogen bond when an arm of one water

molecule aligns with an arm of another water molecule, with an energy function that is a Gaussian function of separation and angle:

$$U_{\mathrm{HB}}(\boldsymbol{X}_i, \boldsymbol{X}_j) = \epsilon_{\mathrm{HB}} G(r_{ij} - r_{\mathrm{HB}}) \sum_{k,l=1}^{3} G(\boldsymbol{i}_k \cdot \boldsymbol{u}_{ij} - 1) G(\boldsymbol{j}_l \cdot \boldsymbol{u}_{ij} + 1) \tag{5}$$

where $G(x)$ is an unnormalized Gaussian function:

$$G(x) = \exp[-x^2 / 2\sigma^2] \tag{6}$$

The unit vector $\mathbf{i}_k$ represents the kth arm on the ith particle (k) 1, 2, 3), and $\mathbf{u}_{ij}$ is the unit vector joining the center of molecule i to the center of molecule j (Figure 1a). H-bonding arms are not distinguished as donors or acceptors; only the degree of alignment of two arms determines the strength of a hydrogen bond.

The model parameters are as defined previously.[40] The parameters $\varepsilon_{\mathrm{HB}} = -1$ and $r_{\mathrm{HB}} = 1$ define the optimal hydrogen bond energy and bond length, respectively. The same width parameter $\sigma = 0.085$ is used for both the distance and the angle deviation of a hydrogen bond. The interaction energy in the Lennard-Jones potential function, $\varepsilon_{\mathrm{LJ}}$, is 1/10 of $\varepsilon_{\mathrm{HB}}$, and the LJ contact distance is 0.7 of that of r_{HB}.[40] Radii for ions are given in units of r_{HB}.

Here, we modified the MB model by including an electrostatic dipole (see Figure 1b). A single negative charge is put at the center of each water molecule, at a distance 0.35 r_{HB} from the surface of the water disk. A single positive charge is put onto one of the H-bonding arms, at a distance 0.165 r_{HB} from the center and 0.185 r_{HB} from the molecule surface. The other two H-bonding arms are uncharged. This position was chosen to match the radius of a Na^+ ion, because sodium ions are found experimentally to cause no change in the entropy of nearby water molecules ($\Delta S_{\mathrm{II}} = 0$).[17]

Several other dipole orientations with two or three charges were also tested. However, the model described here was unique in giving qualitatively correct results for water–water liberation free energies and assumed structuring and was used for further analysis.

An ion interacts with the charges on a water molecule through a screened potential:

$$U_{\mathrm{charge}} = z_i z_j \epsilon_{\mathrm{HB}} a \frac{\exp(-\kappa r_{ij})}{r_{ij}} \tag{7}$$

where r_{ij} is the distance between the ion center and a charge on a water dipole, and the valences z_i (z_j) are +1 or −1. All of the distances are in the units of r_{HB}. Various considerations are involved in choosing this functional form. First, while a logarithmic dependence on r is appropriate for a true 2-D system, our model interactions are chosen to be consistent with three-dimensional Coulomb's law. Our model r^{-1} dependence is appropriate for a two-dimensional slice through a three-dimensional system. Second, following others,[44–47] we use a screened Coulomb potential, rather than a simple Coulombic interaction. We use this for computational efficiency. Several groups have shown that when the properties of interest involve only near-neighbor effects, such as those of interest here, the screened Coulomb potential represents an excellent approximation to the Coulomb potential.[48–51] The parameter $\kappa = 0.1$ is small enough that the interaction potential at short distances would not differ substantially from that of a pure Coulombic potential. Decreasing the screening parameter κ did not influence the results.

The last parameter, $\alpha = 2.27$, is chosen so that when a negative ion with a radius 0.35 r_{HB} (the distance of a negative charge from the surface of a water molecule) or a positive ion with a

radius 0.185 r_{HB} is in its most favorable position relative to a water molecule, the electrostatic energy equals the hydrogen bond energy ($\varepsilon_{HB} = -1$).

The ion–water pair potential is

$$U^{iw}(\boldsymbol{X}_i, \boldsymbol{X}_j) = U_{LJ}(r_{ij}) + \sum_{+,-} U_{charge}(\boldsymbol{X}_i, \boldsymbol{X}_j) \quad (8)$$

The diameter, σ_{LJ}, is different for different ions ($\sigma_{LJ} = (\sigma_{ion} + \sigma_{water})/2$), while the well depth for the Lennard-Jones potential, ε_{LJ}, is taken to be the same for all ions, for simplicity. More realistic models would use different LJ parameters for each ion type.[52] While adding such a parameter is likely to improve our agreement with experiments, our aim here is to develop the simplest model for studying ion charge density effects. This model is also simplified in that the dipole on each water molecule interacts only with ions, not with dipoles on other waters. One of the reasons for using the explicit hydrogen bonds versus a dipole–dipole interaction is its quantum mechanical character which is better treated with the "effective" pair potential.[53] Further, the two-dimensional water models using only an electrostatic interaction were unsuitable for describing the anomalous volumetric properties of water.[54]

Ion sizes in our model were taken from crystal ionic radii.[55] The crystal radii are collected in Table 1, and the model ion sizes are collected in Table 2. The relative sizes were calculated from crystal radii. The conversion factor was determined assuming that the negative proportion of the water molecule used by Collins[27] (r^{neg} = 1.78 Å) corresponds to the MB-dipole water molecule radius, $\sigma/2 = 0.35\ r_{HB}$. Reduced units are used throughout this paper – all energies and temperatures are normalized to the strength of an optimal hydrogen bond energy (e.g., $T^* = k_B T/|\varepsilon_{HB}|$, $U^* = U/|\varepsilon_{HB}|$. Similarly, all distances are scaled by the length of an idealized hydrogen bond (e.g., $V^* = V/r_{HB}^2$). We call this the MB-dipole model.

We studied this model through Monte Carlo simulations in the isobaric (NPT) ensemble.[56] A single (positive or negative) ion was fixed in the center of a simulation box. Monte Carlo steps are displacements and rotations of the water molecules; details are given in ref [40]. The simulations were usually performed on 120 water molecules. The first 10^7 steps were used to equilibrate the system, and then statistics were collected over the following 5×10^8 steps. Pair distribution functions, $g_{ij}(r)$, and thermodynamic properties (energy, enthalpy, volume) were calculated as ensemble averages.[56] In addition, the free energy, enthalpy, and entropy of transferring an ion or a hydrophobe into a solution were calculated using the Widom test-particle method[57] and using related fluctuation formulas.[40] The results were compared to the molar Gibbs free energy, enthalpy, and entropy of hydration and the standard partial molar volume of ions.[55,58] The experimental values are adjusted to correspond the process of ion transfer into the solution studied here as defined by the Ben–Naim standard state.[58]

Because Hofmeister effects are linear in ion concentration[8,9] and because anion and cation effects are generally additive and independent,[8,9] we study Hofmeister effects using a water box that contains a single nonpolar solute and a single ion. We performed model hydrophobe transfers (with a disk of the same size as water molecule, $\sigma = 0.7$) from an isolated phase into equilibrated systems of an ion and 60 water molecules. Hofmeister effects in the MB-dipole model were also calculated by examining the potential of mean force (pmf) between an individual ion and a nonpolar solute at infinite dilution, using the Widom method of Shimizu and Chan.[59] The potential of mean force converged to a value near zero at the largest separations measured and did not require other adjustments to attain values near zero.

3. Results: Water Ordering around Ions

First, we studied the structure of MB-dipole water around ions. Figure 2a and b shows the ion–water pair distribution functions for cations and anions of different sizes. The sizes represent very small (Li^+, F^-), intermediate (Na^+, Cl^-), and large (Cs^+, I^-) ions. These figures show that the smaller ions are bound more closely to water molecules than are larger ions.

Figure 3 shows the angular distributions of first-shell waters around ions. The angle is of a water's dipole vector relative to the vector connecting the water and ion centers. The favored angle is $\theta = 0$ for a water molecule adjacent to an anion, because water points the positive end of its dipole directly at the anion (see Figure 3b). The favored angle is $\theta = 180°$ for a water molecule adjacent to a cation, because water points the positive end of its dipole directly away from the ion (Figure 3a). Figure 3 shows that first-shell waters around an ion are highly oriented, dominated by these preferred orientations.

Figure 3 shows that water orientations result from a balance between this electrostatic ordering mechanism and the water–water hydrogen-bonding ordering mechanism. For the smallest anions (F^- and Cl^-), the electrostatic mechanism dominates: water molecules orient to achieve the most favorable electrostatic orientation with respect to the ion. This is supported by all-atom classical force-field studies of anions in small clusters of water.[60–64] Yet for larger anions (I^-), the first-shell water orientational distribution has two peaks. In that case, water's orientation is a compromise between the electrostatic tendency to orient the dipole with respect to the ion and the hydrogen-bonding tendency to orient two adjacent water molecules in the ion's first shell.

The same balance applies to cations, except that the size tendency is reversed. Figure 3a shows that the large cations (Cs^+) cause a single-peaked and narrow angular distribution of water because the electrostatic tendency is compatible with the hydrogen-bonding tendency in this case. In contrast, the smaller cations lead to double-peaked distributions, implying that the water–water hydrogen bonds are "bending" the dipole angles. Such configurations are also seen in all-atom calculations of intermediate size cation–water cluster structures.[65–68] The exception is the Li^+ water cluster structure[69] which will be discussed in more detail below.

Figure 4 shows the average number of hydrogen bonds made by a water molecule within the first water shell around an ion. This quantity shows the balance between electrostatics and hydrogen bonding. It shows that for the large cations, electrostatics *assists* in the formation of water–water hydrogen bonds, while for all other ions, electrostatics *competes against* hydrogen bond formation. The ions having the highest charge densities (F^-, for example) are the most disruptive of water–water hydrogen bonding. All-atom ion–water simulations show overall breaking of hydrogen bonds (relative to bulk water) in small clusters around ions with high charge density.[70,71] However, in contrast to our MB-dipole model results, hydrogen bond formation is more probable between water molecules clustered around anions than around cations.[71]

Figure 5 summarizes these results. Small cations orient first-shell waters through an electrostatic mechanism, disrupting hydrogen bonding among first-shell waters. Increasing the cation size diminishes the electrostatic force of the ion on the water, leading to increased water–water hydrogen bonding, as would be seen around nonpolar solutes. A similar trend occurs for anions: water structure around small anions is controlled by an electrostatic mechanism, while water structure around larger anions is controlled by hydrogen bonding. A notable difference between anions and cations is the ion size required to achieve a given level of water ordering. Larger anions have the same effect on water ordering as smaller cations. For example, $F^-$and Li^+ affect water ordering to about the same degree even though F^- is a larger ion. This arises in the MB-dipole model, as it does in the Collins hypothesis,[27] from the anisotropic charge

distribution of the water dipole. In its optimal configuration, the + end of a water dipole is about the same distance from the center of a F^- ion as the − end of a water dipole is from the center of a Li^+ ion. This sort of asymmetry is also reflected in the experimental properties, as indicated below.

4. Viscosity Experiments on Chaotropes and Kosmotropes

To test the MB-dipole model against these water structuring experiments, we follow the idea of Chong and Hirata,[72] who proposed that the viscosity enhancement or reduction due to ion effect, as reflected in Samoilov's E_0 and E_i, is proportional to the liberation free energy of stripping a water molecule from an ion's first shell. That is, if there is a large energy barrier to stripping a water away from an ion, it implies that the ion increases water's viscosity. To obtain this quantity, we first calculate the potential of mean force (pmf) between an ion and a water molecule; it is the negative logarithm of the corresponding pair distribution function, $g(r)$. The liberation free energy, G_i^{lib}, is then computed as the difference in the ion–water pmf between the contact minimum and the first peak.[34,72] Liberation free energies are compared to the water–water liberation free energy following Samoilov: $\Delta G_i^{lib} = G_i^{lib} - G_0^{lib}$, where G_0^{lib} is the liberation free energy for a water molecule from another water molecule. Positive ΔG^{lib}'s characterize structure-making ions, and negative ΔG^{lib}'s characterize structure-breaking ions.

Figure 6 compares our computed ΔG^{lib}'s for various ions with three properties: the experimental ΔE_i's of Samoilov,15 experimental ΔS_{II} values, and Jones–Dole B coefficients. The MB-dipole model reproduces well the experimental trends with ion size. ΔG_i^{lib} passes from positive to negative values as the size of the ion increases. The crossover from ordering to disordering in the model occurs around sodium (for cations) and chloride ions (for anions), as it does in the experiments. Our model simulations for ΔG^{lib} for divalent cations are also in good agreement with the experiments. The higher liberation free energies are due to the higher charge densities of multivalent ions than those of monovalent ions.

Figure 7 shows that ionic effects on water ordering can be described by a universal curve based on the charge density of the ion. In Figure 7, ΔG_i^{lib} is plotted against the radii of the anions, while the curves for cations were shifted by a constant distance that approximately corresponds to asymmetry in the water dipole. The cation and anion that were used for the estimation were the two determining the line between chaotropes and kosmotropes: Na^+ and Cl^- for ΔS_{II} and ΔG^{lib}, and K^+ and Cl^- for Jones–Dole B coefficient and ΔE_i of Samoilov. Figure 7 shows that the degree of water ordering by cations and anions depends principally on the asymmetry of the water dipole with respect to the water center.

We also calculated ΔG^{lib}'s for multiatom ions. While the experimental data[15,17,18] for multiatom ions give a slightly different correlation with charge density, calculations for our MB-dipole model do not exhibit such trends. This may be due to differences in dispersion interactions and more complex charge distributions,[17] not treated by the uniform LJ parameters in our current model.

5. Modeling the Thermodynamics for Transferring Ions into Water

We computed thermodynamic properties for transferring an ion from the gas phase into aqueous solution using the Widom insertion method.[40] Despite the well-known problems of the Widom method due to insufficient sampling of high energy configurations (ionic solutes), we found the 2-D systems studied here small enough to obtain reliable statistics for ΔG, ΔH, and ΔS of ion solvation. To test the accuracy of the results, the interaction energy obtained from the Widom insertion method was compared with the ion–water interaction energy obtained as an ensemble average from the Monte Carlo simulation. The values were identical

within the statistical error. The method was not accurate enough to obtain heat capacities from fluctuations in ΔH.

Results are compared with experiments in Table 2. The model Gibbs free energies of ion hydration, ΔG_i^{hyd}, give the same trends as the experiments:[58] (1) Smaller ions have the most favorable insertion free energies. (2) The free energies are dominated by the enthalpies. (3) Comparing anions to cations, lithium is approximately equivalent to fluoride.

For all ions, computed ion hydration enthalpies are negative and increase with ion size, in agreement with experiments.[55] To make a more quantitative comparison between our 2-D model and 3-D experiments, we divided the experimental enthalpies by their ion hydration numbers[60] and divided our theoretical results by the number of water molecules in the first hydration shell. The results are collected in Tables 1 and 2. Ion–water enthalpies grow more positive with increasing ion size because the electrostatic interaction with water weakens for larger ions.

Table 2 also gives the computed entropies of ion hydration, which can be compared with the experimentally obtained values in Table 1. As noted above, smaller ions cause greater water ordering. For both cations and anions, the entropies of hydration increase with ion size as observed experimentally. This can also be explained in terms of charge density. Bigger ions have smaller charge density so they bind water molecules less tightly and therefore cause less restriction of water conformations. Thus, the experimental entropies of ion hydration grow less negative for larger ions. For the model, this is observed for the anions, but not for the cations.

6. The Temperature Dependence of Chaotropic and Kosmotropic Effects

Figure 8 compares the temperature dependences of the computed model liberation free energies with the experimental Jones–Dole *B* viscosity coefficients.[17] For all of the cations and most of the anions, the model predicts that heating cold aqueous solutions increases the relative ordering of first-shell waters by an ion, in agreement with experiments. This is explained in the model as follows. The electrostatic ordering of water by an ion is not strongly dependent on temperature. Yet heating pure cold water in the bulk breaks water–water hydrogen bonds. Hence the difference (the liberation free energy of water from an ion minus the liberation free energy of water from water) indicates more relative ordering of waters around an ion than around a water molecule, with increasing temperature. Figure 9 shows the change in electrostatic binding energy and the number of water–water hydrogen bonds with increasing temperature. The figure shows that, except for fluoride, the electrostatic energy decreases less steeply with temperature than the number of hydrogen bonds decreases with temperature.

Figure 8 shows an incorrect prediction of the model: experiments show that the Jones–Dole *B* coefficient for lithium decreases with temperature, while the model predicts an increase with temperature. This may be a result of more structure around lithium ions than the MB-dipole model predicts. It is known from all-atom simulations[69] that lithium ions have a well-defined first hydration shell of four water molecules arranged with tetrahedral symmetry. Each of these four water molecules is bonded to three other water molecules in the second hydration shell. The fourth binding site of each first-shell water molecule is occupied by the central lithium ion itself.[69] This specific solvation structure may break down with increasing temperature, leading to the experimentally observed negative slope for the *B* coefficient that is not captured in the model.

7. Hofmeister Effects

How do different salts affect the solubilities of nonpolar solutes in water? To explore this, we transferred a hydrophobe into an ion–water solution and also transferred the hydrophobe into

pure water. We computed the difference in free energy Δ-(ΔG). This quantity was compared with the experimental salting-out constants for benzene.[29,31] All of the cations and anions studied here predict salting-out of the hydrophobe (positive k_s). Small ions strongly salt-out hydrophobes. Larger ions have a smaller effect. The results are shown in Table 3 and in Figure 10.

In our model, the Hofmeister effect occurs by the following mechanism. At the high salt concentrations that are relevant for the Hofmeister series, the hydrophobe inserts either into the first water shell around the ion or into the second water shell (see Figures 11 and 12). Small ions bind water tightly, so the hydrophobe is excluded from their first solvation shell. This increases the hydrophobe concentration in the "remaining space" (not occupied by ions or their solvation-shell waters), leading to salting-out of the hydrophobes. Larger ions lead to less salting-out because they do not bind waters so tightly in their solvation shells, so they do not exclude hydrophobes from their solvation shells so effectively. This mechanism is consistent with cosolute exclusion, the preferential exclusion of cosolute ions and molecules from hydrophobic sites.[9,32,33]

In these simulations, neither the ion–water pair distribution functions nor the angular orientation of water molecules around ions change significantly in the presence of a hydrophobe (Figure 11). The hydrophobe–water pair distribution function did not change significantly near ions (not shown here). Although the solute–water correlation functions contribute to the solution properties, the most significant contributions can be related directly to the measured ion–solute correlations.

In real systems, very large ions can cause salting-in, that is, increased solubility of nonpolar solutes relative to pure water. In MB water, this does not happen. This is because large ions often have hydrophobic substituents with an added attraction for nonpolar solutes,[74] an interaction which we have not included here.

The MB-dipole model fails to reproduce lithium's position in the Hofmeister series. Lithium is very small and causes a high degree of electrostriction of water in the MB-dipole model. In contrast, experiments show that lithium salts-out benzene less than would be expected based on its high charge density (see Figure 10a and Figure 7). One clue to understanding the Hofmeister effect of lithium is that while it has a large surface charge density, its surface waters are actually *less* electrostricted than sodium's.[29] Lithium's larger than expected molar volume is probably due to lithium's tetrahedral coordination of water.[69] Given its large charge density, lithium would be expected to strongly perturb water structure, but instead it enhances tetrahedral coordination. In general, Hofmeister effects are more closely related to experimental ion solvation volumes than to charge densities.[29,73] The same is true for the MB-dipole model (Figure 10c), hence the conclusion above that the primary Hofmeister mechanism is hydrophobe exclusion from the volume occupied by the ion and its first solvation shell.

8. Justification of the Model

A question can be raised about the physical basis for our model. The principal issue is our use of the electrostatic energy only for water–ion interactions and not for water–water interactions. It is the "canonical view" that water's charges should be universally applied to all charge interactions: with ions or with other waters. However, we believe that our strategy not only has advantages, but also, upon deeper inspection, is arguably no less physical than the canonical strategy.

What is the physical justification? Certainly the "gold standard" for physical correctness would be a quantum mechanical treatment of ion–water and water–water interactions. The canonical

view as described above rests on traditional thinking that is embodied in classical force fields, which, of course, are based on many approximations to the true underlying quantum mechanics: (1) neglect of polarizabilities, (2) approximating the charge multipoles by fixed point charges, (3) approximating the true wave function as a sum of four power-law terms: r^{-1} (charge–charge, ion–water), r^{-3} (dipole–dipole, water–water), and r^{-6} and r^{-12} (van der Waals, for both ions and water), where the exponents 3 and 6 are valid only asymptotically at large r, and 12 is chosen for computational convenience. In short, the true quantum mechanical wave function is approximated as a sum of four terms with exponents 1, 3, 6, and 12, where the 1 and 3 terms are taken to have a common coefficient based on assuming fixed charges. In the canonical strategy, all of the variances among ions of a given valence are captured through the van der Waals parameters: the r^{-12} term handles ionic size, and the r^{-6} term handles the short-ranged ionic interactions. In this canonical strategy, there are two parameters describing the short-ranged behavior of each ion type. This sort of strategy is now so common that it is taken for granted as being “physically correct”. Of course, it is not physically correct. It is a concatenation of assumptions and approximations to deeper quantum mechanical models.

What is our strategy instead? Our strategy also parses the wave function into four terms, but they are different ones: r^{-12} (size), r^{-6} (neighbor attractions), Gaussian (water–water H-bonds), and a Yukawa potential, e^{-r}/r (ion–water). There is no reason to believe that this parsing of the wave function is any less physical than the canonical parsing, particularly because our interest here is only in short-ranged interactions, where Gaussians and Yukawa functions undoubtedly better capture the spirit of atomic orbitals than do classical power laws.

Yet, in addition, our model has some advantages. First, ours has fewer parameters. Instead of two parameters per ion, we have one size parameter per ion, plus one attraction parameter for all anions and one attraction parameter for all cations. For the present kind of model, which is already highly simplified, fewer parameters and greater simplicity are paramount. There is an advantage in having the fewest possible free parameters. The second advantage is that our strategy allows us to retain a simplest possible model for pure water and hydrophobic effects, containing no charge-related parameters. That is, pure water or hydrophobic effects are treated by the MB model, for which all interactions are short-ranged. Only for water containing ions do we then need to introduce the longer-ranged electrostatic interactions of the present model. In this way, interpreting the properties of the pure water and hydrophobicity is simpler than it would have been with the present model, for which charges would have added unwarranted complexity, in our view.

The main point is that the concept of universal charges is not an issue of physics; it is an issue of parametrization in approximate models. We regard our strategy as having a physical basis that is as sound as any canonical strategy that requires common charge parameters in the 1 and 3 terms.

9. Conclusions

We have developed a simple statistical mechanical model to study how ions affect the structure of neighboring water molecules. We used the two-dimensional MB model, modified by the addition of an electric dipole. We show that this model explains the main solvation properties of ions, their chaotropic and kosmotropic effects, as reflected in the Jones–Dole B coefficients of the viscosity increments of water by ions, ion solvation thermodynamics, and the Hofmeister series of ion effects on nonpolar solubilities in water. The model predicts that small ions cause a high degree of electrostatic ordering of neighboring waters. For larger ions, electrostatic effects are smaller, so water structure is dominated by water–water hydrogen bonding in the first shell around the ion. We believe these physical ideas translate directly to understanding three-dimensional water and that the reduced dimensionality of the present model is not a

serious hindrance to general physical insights into the processes by which ions order neighboring water molecules.

Acknowledgements

We are grateful for support from NIH grant GM 34993 to K.A.D., and a UCSF Graduate Dean Fellowship to N.T.S. We appreciate the support of the North Atlantic Treaty Organization under a grant awarded in 1999 (PST.CLG 974882). Part of the material is based upon work supported by the North Atlantic Treaty Organization under a grant awarded to B.H. in 2000.

References

1. Dill KA. Biochemistry 1990;29:7133–7155. [PubMed: 2207096]
2. Rupley J, Careri G. Adv Protein Chem 1991;41:37–172. [PubMed: 2069077]
3. Chalikian TV, Volker J, Plum E, Breslauer K. Proc Natl Acad Sci USA 1999;96:7853–7858. [PubMed: 10393911]
4. Sussman F, Weinstein H. Proc Natl Acad Sci USA 1989;86:7880–7884. [PubMed: 2813364]
5. Lybrand TP, McCammon A, Wiff G. Proc Natl Acad Sci USA 1986;83:833–835. [PubMed: 3456569]
6. Jordan PC. Biophys J 1990;58:1133–1156. [PubMed: 1705448]
7. Katz, B. Nerve, Muscle, and Synapse; McGraw-Hill: London, 1966.
8. Collins KD, Washabaugh MW. Q Rev Biophys 1985;18:323–422. [PubMed: 3916340]
9. Cacace MG, Landau EM, Ramsden JJ. Q Rev Biophys 1997;30:241–277. [PubMed: 9394422]
10. Maroncelli M, MacInnins J, Fleming GR. Science 1989;243:1674–1681. [PubMed: 17751278]
11. Kropman MF, Bakker HJ. Science 2001;291:2118–2120. [PubMed: 11251110]
12. Larwood VL, Howlin BJ, Webb GA. J Mol Model 1996;2:175–182.
13. Habuchi S, Kim HB, Kitamura N. Anal Chem 2001;73:366–372. [PubMed: 11199991]
14. Chavez-Paez M, Van Workum K, de Pablo L, de Pablo LL. J Chem Phys 2001;114:1405–1413.
15. Samoilov OY. Discuss Faraday Soc 1957;24:141–146.
16. Samoilov, O. Y. In Water and Aqueous Solution: Structure, Thermodynamics, and Transport Processes; Horne, R. A., Ed.; Wiley-Interscience: New York, 1972; pp 597–612.
17. Krestov, G. A. Thermodynamics of Solvation; Ellis Horwood: New York, 1990.
18. Robinson, R. A.; Stokes, R. H. Electrolyte Solutions; Butterworth Scientific Publications: London, 1959.
19. Bernal JD, Fowler RH. J Chem Phys 1933;1:515–548.
20. Marx D, Sprik M, Sprik M, Parinello M. Chem Phys Lett 1997;273:360–366.and references therein.
21. Heinzinger K, Vogel PC. Z Naturforsch 1974;A29:1164–1171.
22. Galli, G.; Parrinello, M. In Computer Simulations in Materials Science; Meyer, M., Pontikis, V., Eds.; Kluwer: Dordrecht, 1991.
23. Payne MC, Teter MP, Allan DC, Arias TA, Joannopoulos JD. Rev Mod Phys 1992;64:1045–1097.
24. Galli, G.; Pasquarello, A. In Computer Simulations in Chemical Physics; Allen, M. P., Tildesley, D. J., Eds.; Kluwer: Dordrecht, 1993.
25. Hummer G, Pratt LR, Garcia AE. J Phys Chem A 1998;102:7885–7895.
26. Kaminsky M. Discuss Faraday Soc 1957;24:171–179.
27. Collins KD. Biophys J 1997;72:65–76. [PubMed: 8994593]
28. Hofmeister F. Arch Exp Pathol Pharmakol 1888;24:247–260.
29. McDevit WF, Long FA. J Am Chem Soc 1952;74:1773–1777.
30. von Hippel PH, Schleich T. Acc Chem Res 1969;2:257–265.
31. Baldwin RL. Biophys J 1996;71:2056–2063. [PubMed: 8889180]
32. Smith PE. J Phys Chem B 1999;103:525–534.
33. Kalra A, Tugcu N, Cramer S, Garde S. J Phys Chem B 2001;105:6380–6386.
34. Kalyuzhnyi, Yu V, Vlachy V, Dill K. Acta Chim Slov 2001;48:309–316.

35. Eisenberg, D.; Kauzmann, W. The Structure and Properties of Water; Oxford University Press: Oxford, 1969.
36. Franks, F., Ed. Water, A Comprehensive Treatise; Plenum Press: New York, 1972–1982; Vols. 1–7.
37. Stillinger FH. Science 1980;209:451–457. [PubMed: 17831355]
38. Zhu SB, Singh S, Robinson GW. Adv Chem Phys 1994;85:627–731.
39. Robinson, G.; Zhu, S. B.; Singh, S.; Evans, M. Water in Biology, Chemistry, and Physics: Experimental Overviews and Computational Methodologies; World Scientific: Singapore, 1996.
40. Silverstein KA, Haymet ADJ, Dill KA. J Am Chem Soc 1998;120:3166–3175.
41. Tanford, C. The Hydrophobic Effect: Formation of Micelles and Biological Membranes; Wiley: New York, 1980.
42. Ben-Naim, A. Hydrophobic Interactions; Plenum Press: New York, 1983.
43. Southall NT, Dill KA. J Phys Chem B 2000;104:1326–1331.
44. Hassan SA, Guarnieri F, Mehler EL. J Phys Chem B 2000;104:6478–6489.
45. Ferreira PG, Dymitrowska M, Belloni L. J Chem Phys 2000;113:9849–9862.
46. Bhattacharya A, Mahanti SD. J Phys: Condens Matter 2001;13:1413–1428.
47. Hassan SA, Mehler EL. Int J Quantum Chem 2001;183:193–202.
48. Larsen B, Rodge SA. J Chem Phys 1980;72:2578–2586.
49. Rodge SA, Hafskjold B. Acta Chem Scand 1981;A35:263–273.
50. Leote de Carvalho RJF, Evans R. Mol Phys 1997;92:211–228.
51. Hribar B, Vlachy V. Langmuir 2001;17:2043–2046.
52. Hummer G, Pratt LR, Garcia AE. J Phys Chem 1996;100:1206–1215.
53. Ben-Naim, A. Water and Aqueous Solutions; Plenum Press: New York, 1974.
54. Okazaki K. J Chem Phys 1981;75:5874–5884.
55. Marcus, Y. Ion Solvation; Wiley-Interscience: New York, 1985.
56. Allen, M. P.; Tildesley, D. J. Computer Simulation of Liquids; Oxford University Press: Oxford, 1987.
57. Widom B. J Chem Phys 1963;39:2808–2812.
58. Marcus Y. Biophys Chem 1994;51:111–127.
59. Shimizu S, Chan HS. J Am Chem Soc 2001;123:2083–2084. [PubMed: 11456842]
60. Lee SH, Rasaiah JC. J Phys Chem 1996;100:1420–1425.
61. Xantheas SS, Dang LX. J Phys Chem 1996;100:3989–3995.
62. Bryce RA, Vincent MA, Malcolm NOJ, Hillier IH. J Chem Phys 1998;109:3077–3085.
63. Sremaniak LS, Perera L, Berkowitz ML. J Phys Chem 1996;100:1350–1356.
64. Ayala R, Martinez JM, Pappalardo RR, Marcos ES. J Phys Chem A 2000;104:2799–2807.
65. Kollman PA, Kuntz ID. J Am Chem Soc 1972;94:9236–9237.
66. Kollman PA, Lybrand T, Cieplak P. J Chem Phys 1988;88:8017.
67. Caldwell JW, Kollman PA. J Phys Chem 1992;96:8249–8251.
68. Ramaniah LM, Bernasconi M, Parinello M. J Chem Phys 1999;111:1587–1591.
69. Lyubartsev AP, Laasonen K, Laaksonen A. J Chem Phys 2001;114:3120–3126.
70. Combariza JE, Kestner NR. J Phys Chem 1995;99:2717–2723.
71. Topol IA, Tawa GJ, Burt SK, Rashin AA. J Chem Phys 1999;111:10998–11014.
72. Chong SH, Hirata F. J Phys Chem B 1997;101:3209–3220.
73. Wen-Hui X, Jing-Zie S, Xi-Ming X. Thermochim Acta 1990;169:271–286.
74. Desnoyers JE, Pelletier GE, Jolicoeur C. Can J Chem 1965;43:3232–3237.

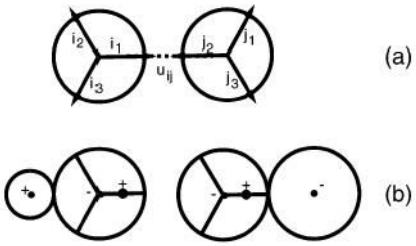

Figure 1.
The MB-dipole model. (a) Two MB-dipole waters forming a hydrogen bond. (b) A cation and an MB-dipole water oriented in its most favorable orientation (180° with respect to the vector connecting the molecular centers). Also an anion and a water oriented in its most favorable orientation (0°).

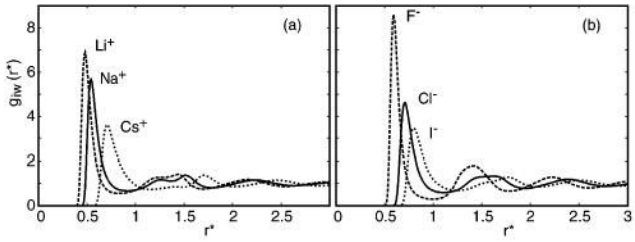

Figure 2.
Pair correlation functions of water around ions. (a) Cations and (b) anions. Smaller ions have tighter water shells, at reduced temperature $T^* = 0.20$.

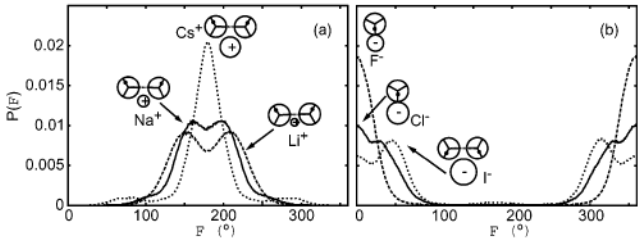

Figure 3.

Angular distribution functions for waters in the first shell around an ion, for (a) cations and (b) anions at $T^* = 0.20$. Large cations help promote hydrogen bonding of neighboring waters, leading to a single peak. For small cations, the electrostatic mechanism competes with the hydrogen bond mechanism for ordering waters. The reverse applies to anions. For small anions, the electrostatic mechanism dominates; for large anions, electrostatic and hydrogen-bonding mechanisms compete.

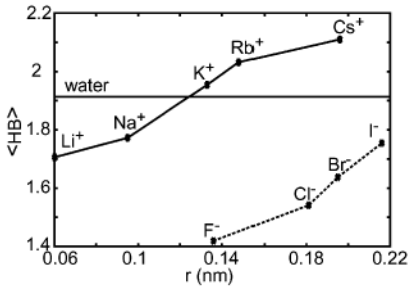

Figure 4.
The average number of the water–water hydrogen bonds, ⟨HB⟩, per water molecule in the first shell around various ions at $T^* = 0.20$.

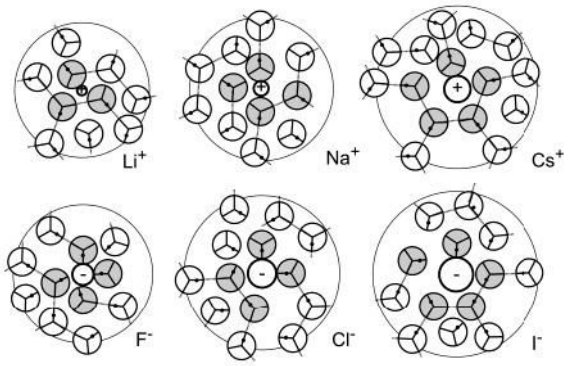

Figure 5.
Snapshots of waters in the first (shaded) and second shell (white) around an ion (black), showing likely configurations of water as inferred from statistics of pair distributions, angular orientations, and hydrogen bonding at $T^* = 0.20$.

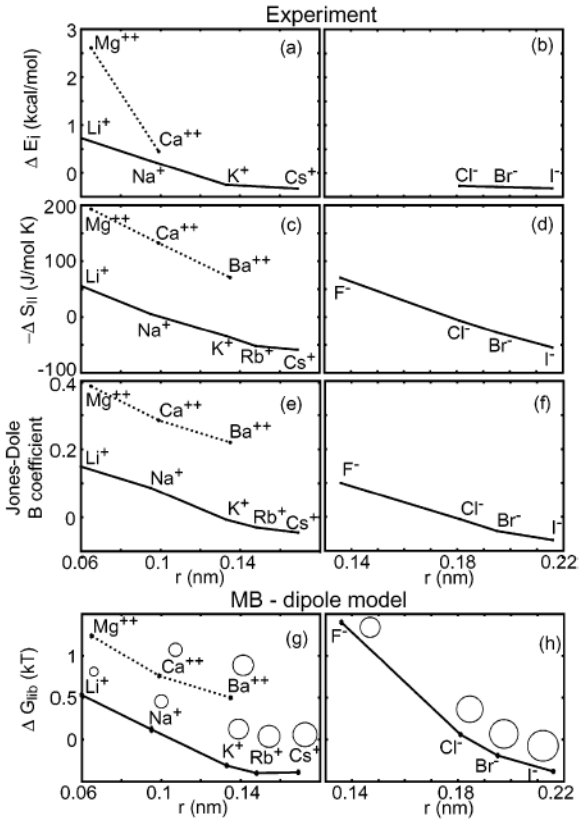

Figure 6.

The MB-dipole model reproduces the dependence on ion radius of chaotropic and kosmotropic properties. The activation energy of Samoilov, ΔE_i (ref 15), changes in entropy, $-\Delta S_{II}$ (ref 17), and Jones–Dole *B* coefficients (ref 18), all at 298 K, are compared to the MB-dipole model liberation free energy, ΔG^{lib}, at $T^* = 0.20$. σ for Mg^{++}, Ca^{++}, and Ba^{++} was taken to be 0.26, 0.39, and $0.53 l_{HB}$, scaled from ionic crystal radii.[55] Zero values indicate the transition between kosmotropes (greater than zero) and chaotropes (less than zero). Circles indicate relative ion radii.

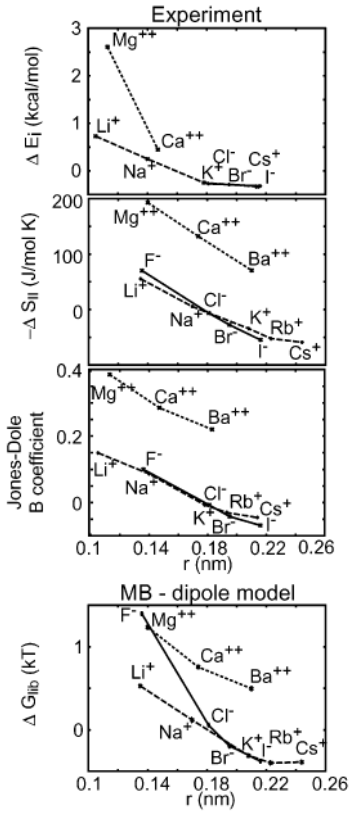

Figure 7.

A universal curve showing that chaotropic and kosmotropic properties depend on electrostatic potential at the ion. The activation energy of Samoilov, ΔE_i (ref 15), changes in entropy, ΔS_{II} (ref 17), and Jones–Dole *B* coefficients (ref 18), all at 298 K, as compared to the MB-dipole model liberation free energy, ΔG^{lib}, are shown for sets of cations and anions at $T^* = 0.20$. A single distance shift was chosen to overlay the cations onto the anions, indicating that the physical basis for this asymmetry is the asymmetry of the dipole in water.

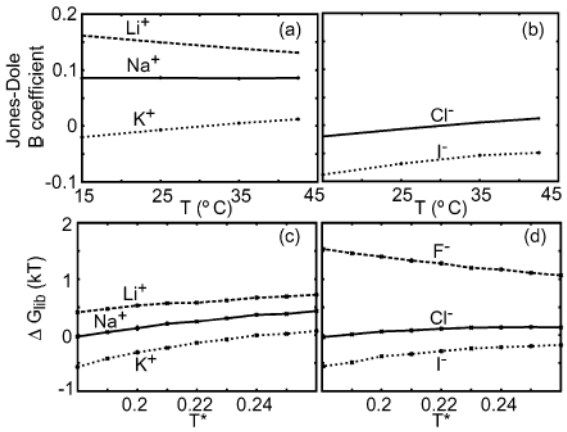

Figure 8.

The MB-dipole model reproduces the temperature dependence of chaotrope and kosmotrope behavior. The temperature dependence of Jones–Dole viscosity coefficients, $B(T)$, from experiments[18] for (a) cations and (b) anions, and the temperature dependence of liberation free energy, ΔG^{lib}, from the MB-dipole simulations for (c) cations and (d) anions are shown.

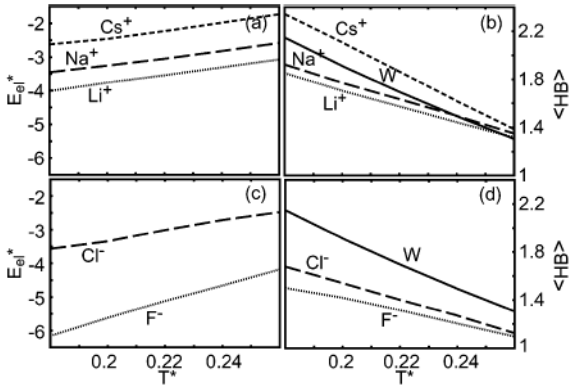

Figure 9.

The temperature dependence of electrostatic energy, E^{elec}, and the number of hydrogen bonds per molecule in the first shell, n_{HB}/n_{shell}, for cations (a and b) and anions (c and d).

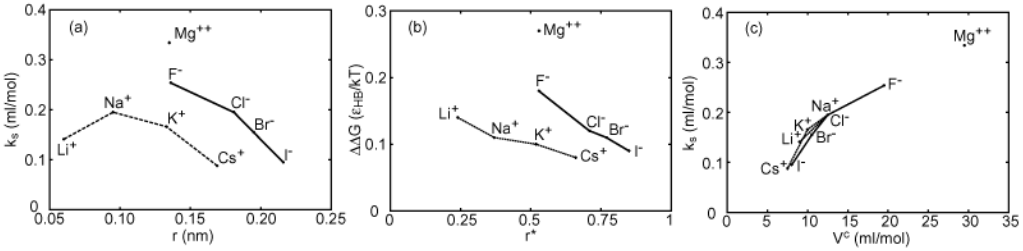

Figure 10.

Hofmeister effects in water and the MB-dipole model. (a) Experimental Setschenow coefficients for cation-chloride and sodium-anion salts as a function of ionic radii. (b) Perturbations to the free energy of transferring a hydrophobic solute into MB-dipole water with an ion, $\Delta\Delta G$. (c) Experimental correlation between compression volumes for salts[29] and Setschenow coefficients. Salts shown as in (a).

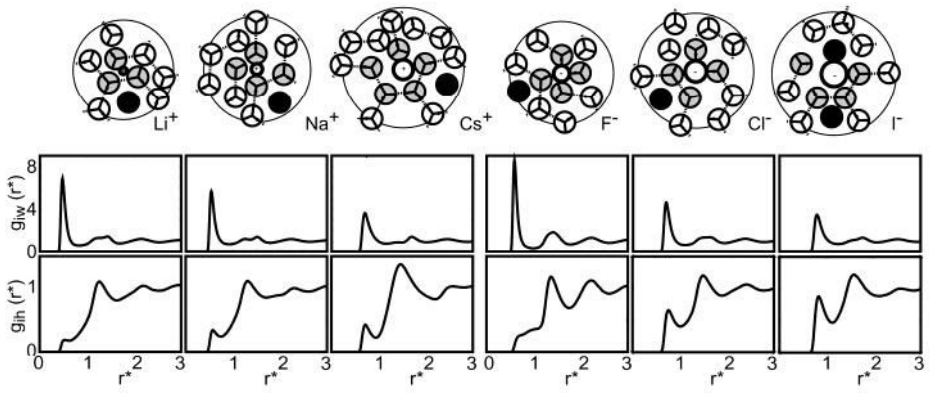

Figure 11.

Water density around an ion affects the probability of hydrophobic solute insertion and the magnitude of Hofmeister effects. Shown are (top) most probable sites of hydrophobic solute insertion (colored black) in the first and second shell around different ions, measured in MB-dipole simulations. (middle) The average water density around different ions at $T^* = 0.20$. (bottom) The potential of mean force between an ion and a hydrophobe at $T^* = 0.20$ showing that solute insertion is favorable when first-shell water density decreases.

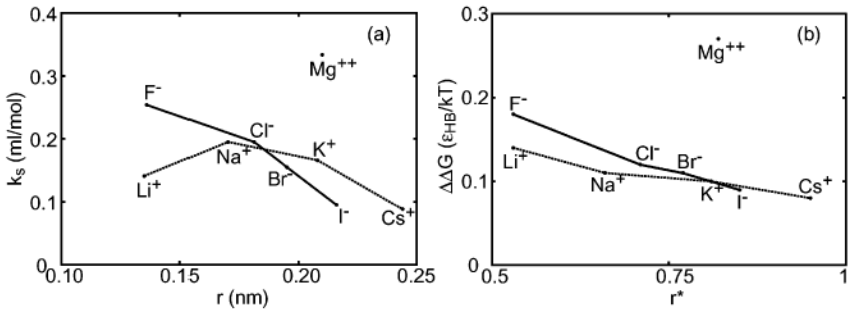

Figure 12.

"Universal" charge density correlation for Hofmeister effects. Shown are (a) experimental Setschenow coefficients versus ionic radii, adjusting cation radii by 0.075 nm as in Figure 7, and (b) MB-dipole $\Delta\Delta G$ for ion effects on hydrophobic solute transfer free energies.

Table 1

The Crystal Ionic Radii, and Experimentally Obtained Thermodynamics of the Ion Solvation[a]

ion	r_M	hydration number	ΔG^{hyd}	ΔH^{hyd}	ΔS^{hyd}
Li^+	0.060	4.1	−116	−129	−32
Na^+	0.095	5.9	−62	−70	−22
K^+	0.133	7.2	−41	−46	−13
Rb^+	0.148	7.8	−35	−39	−11
Cs^+	0.169	9.6	−26	−29	−8
F^-	0.136	6.4	−73	−80	−24
Cl^-	0.181	7.4	−46	−49	−13
Br^-	0.195	7.2	−44	−47	−11
I^-	0.216	8.1	−34	−36	−7

[a] Shown are the crystal ionic radii, r_M,[55] with the experimentally obtained thermodynamics of the ion solvation: change of Gibbs free energy, ΔG^{hyd}, enthalpy, ΔH^{hyd}, and entropy, ΔS^{hyd}, of hydration[58] per first-shell water molecule. Hydration numbers are taken from ref [60]. Ion radii are given in nanometers, ΔG^{hyd} is in units of kJ/mol/hydration number, ΔH^{hyd} is in kJ/mol/hydration number, and ΔS^{hyd} is in J/K/hydration number.

Table 2

Ion Diameters Used in the MB-Dipole Model, and Ion Insertion Thermodynamics into MB-Dipole Water[a]

ion	σ	hydration number	ΔG^{hyd}	ΔH^{hyd}	ΔS^{hyd}	E^{el}
Li^+	0.24	3.29	−16.01 ± 0.04	−30.2 ± 0.2	−24.2 ± 0.3	−28.59 ± 0.07
Na^+	0.37	3.50	−12.09 ± 0.06	−24.7 ± 0.3	−21.6 ± 0.5	−23.25 ± 0.07
K^+	0.52	4.01	−8.22 ± 0.03	−19.4 ± 0.4	−19.1 ± 0.6	−17.8 ± 0.1
Rb^+	0.58	4.38	−6.82 ± 0.03	−17.5 ± 0.4	−18.2 ± 0.8	
Cs^+	0.66	4.53	−5.78 ± 0.03	−16.5 ± 0.5	−18.2 ± 0.7	−14.25 ± 0.05
F^-	0.53	4.12	−14.1 ± 0.1	−25 ± 3	−18 ± 4	−31.9 ± 0.1
Cl^-	0.71	4.35	−7.78 ± 0.08	−16 ± 2	−13 ± 4	−18.99 ± 0.06
Br^-	0.77	4.55	−6.4 ± 0.1	−13 ± 1	−11 ± 2	−16.28 ± 0.05
I^-	0.85	4.83	−4.62 ± 0.03	−10.8 ± 0.4	−10.5 ± 0.7	−13.5 ± 0.1

[a] Shown are ion diameters used in the MB-dipole model, σ, and the change in Gibbs free energy, ΔG^{hyd}, enthalpy, ΔH^{hyd}, entropy, ΔS^{hyd}, and electrostatic energy, ΔE^{el}, per first-shell water molecule, for ion insertion in MB-dipole water, as obtained from the Widom insertion method at $T^* = 0.20$. Ion radii are given in reduced units for the MB-dipole model. ΔG^{hyd}, ΔH^{hyd}, and ΔS^{hyd} have the same units as in Table 11, assuming ε_{HB} in the MB-dipole model has an energy of 24.37 kJ/mol.[53]

Table 3

Experimental Solvent Compression Volumes[a]

ion	experiment		model	
	ΔV^c (cm^3/mol)	(dm^3/mol) k_s	ΔV (V^*)	$\Delta(\Delta G)$ (ε_{HB}/kT)
Li^+	9.0	0.141	−1.18	0.14
Na^+	12.5	0.195	−1.04	0.11
K^+	10.0	0.166	−0.38	0.10
Cs^+	7.5	0.088	−0.08	0.08
Ba^{2+}	29.5	0.334	−2.17	0.27
F^-	19.5	0.254	−1.38	0.18
Cl^-	12.5	0.195	−0.47	0.12
Br^-	10.5	0.155	−0.08	0.11
I^-	8.0	0.095	2.32	0.09

[a]The experimental solvent compression volumes, ΔV^C ($\Delta V^C = V_S - \overline{V}_{s0}$, where V_S is the liquid volume of the pure salt, and $\overline{V}_{s0}$ is the partial molar volume of the salt at infinite dilution in water), and salting-out constants for benzene in the presence of different salts, k_S,29 as compared with the MB-dipole model partial molar volumes, ΔV, and $\Delta(\Delta G)$ for hydrophobe transfer in the MB-dipole model in the presence of different ions. The values of ΔV^C and k_S are not given for single ions but for salts – chloride (for cations) and sodium (for anions).